Struct Multidisc Optim 23, 75–87

A finite element optimization technique to determine critical imperfections of shell structures

A.A. El Damatty and A.O. Nassef

Abstract Geometric imperfections play a significant role in the evaluation of the buckling capacity of thin-walled structures. Since the pattern and distribution of such imperfections take a random variation, the determination of a critical imperfect shape that leads to the minimum buckling load becomes a challenge. In this study, an optimization technique based on binary coded genetic algorithms is used together with a nonlinear finite element model to identify the critical imperfection pattern for thin-walled welded structures. The finite element model is based on a consistent sub-parametric shell element that accounts for the effect of both geometric and material nonlinearities. The binary coded genetic algorithm is used as the optimization means to arrive at the imperfection pattern leading to the near globally minimum buckling load. A previously developed mathematical model is employed to describe the imperfection bulges associated with lines of weldment. The method is demonstrated by considering the nonlinear stability analysis of both a circular cylinder subjected to pure axial compressive load and a conical tank under hydrostatic pressure. The combined genetic algorithm – finite element code is used to determine the critical imperfection bulge patterns for the two problems, as well as their associated buckling loads.

Key words shell structures, genetic algorithms, buckling, welding imperfections, finite elements, optimization

Received September 29, 2000
Revised manuscript received April 20, 2001

A.A. El Damatty[1] and A.O. Nassef[2]

[1] Department of Civil and Environmental Engineering, University of Western Ontario, London, Ontario, N6A 5B9, Canada
e-mail: damatty@uwo.ca
[2] Mechanical Design and Production Department, Faculty of Engineering, Cairo University, Cairo, 12613, Egypt
e-mail: aosama@alpha1-eng.cairo.eun.eg

1 Introduction

Thin-walled structures (e.g. tanks and pressure vessels) are usually constructed by welding curved metal panels. As a result of the welding process, a geometric depression (bulge) can occur along the line of weldment. Based on extensive experimental measurements, Rotter and Teng (1989) have identified the typical bulges that might develop along the weldment line for large-scale shell structures. In the same study, mathematical expressions for these typical bulges were suggested. In practice, along a line of weldment, a bulge might or might not occur depending on the quality of the welding process in the specified location. As such, the imperfections associated with a certain welding configuration can have a very large number of possible patterns.

The buckling capacity of thin-walled structures is greatly affected by the initial imperfection pattern existing in the structure. The purpose of this study is to develop a technique that predicts the critical distribution of bulges that might occur for a given welding configuration and leads to the minimum buckling capacity of the structure. The technique involves coupling between a finite element model and a binary coded genetic algorithm. The study starts by describing the possible imperfection patterns that might be associated with a welding configuration of a thin-walled structure. This is followed by a description of the optimization technique that is used to determine the imperfection pattern associated with the minimum buckling load. For the purpose of demonstration, two examples that involve nonlinear stability analysis of thin-walled structures are then presented. In these examples, the critical imperfection patterns and their associated buckling loads are determined for a hydrostatically loaded conical tank and for a cylinder subjected to a pure axial compression load.

2 Imperfection patterns for thin-walled structures

A part of a thin-walled structure is shown in Fig. 1. It consists of a number of curved panels that are welded to-

gether using one circumferential weld (H1) as well as four meridional welds (V1, V2, V3 and V4). Along each line of weldment, imperfections (bulges) might occur as a result of the welding process.

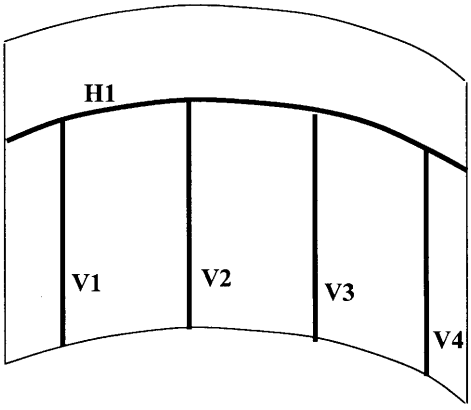

Fig. 1 Lines of weldment for a thin-walled structure

Rotter and Teng (1989) have conducted a large number of field measurements to determine the shape of typical weld depressions. Based on this study, two mathematical models that describe the weld depression were suggested. These were labelled as types A and B as shown in Fig. 2.

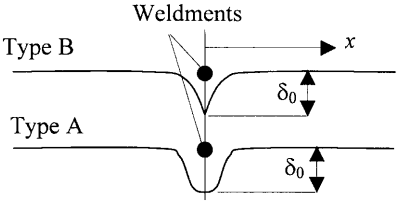

Fig. 2 Types of bulge depression due to welding

The profile of types A and B bulges are given by (1) and (2), respectively,

$$\delta(x) = \delta_0\, e^{-\pi x/\lambda} \left(\cos\frac{\pi x}{\lambda} + \sin\frac{\pi x}{\lambda}\right), \tag{1}$$

$$\delta(x) = \delta_0\, e^{-\pi x/\lambda} \cos\frac{\pi x}{\lambda}, \tag{2}$$

$$\lambda = \frac{\pi\sqrt{Rt}}{[3(1-\nu^2)]1/4}, \tag{3}$$

where δ_0 is the amplitude of the depression (bulge), R is the radius of the cross-section of the thin-walled structure, t is the thickness, ν is Poisson's ratio and λ is the imperfection's half wavelength. It should be noted that the weld depression has an inward direction, i.e. it is directed toward the axis of revolution of the shell.

For each weld line (H1, V1, V2, V3 and V4), bulges in the form of types A or B can occur either along the whole length of the weldment line or at combinations of certain discrete locations along each line. The geometry of the shell structure, associated with a certain imperfection configuration, is modelled in this study using nonuniform rational B-Splines (NURBS).

The occurrence, or non-occurrence, of weld imperfections can be modelled by discretizing the weld lines into a number of equally spaced segments, then by pulling the points along the segment with displacements obtained from (1) or (2) on a path normal to the structure's surface. An engineering decision is taken to choose the number of different bulges configurations (segments) for both the meridional (n) and circumferential (m) lines of weld. It is clear that the larger the values of n and m, the more accurate the results of the analysis. However, an increase in the values of m and n would lead to significant increase in the computational time. For demonstration, let $n = 3$ and $m = 8$. For such a case, the maximum value of the bulges can occur independently at axes A, B and C (Figs. 3–6) for the meridional welds, and along segments 1 to 8 for the circumferential weld.

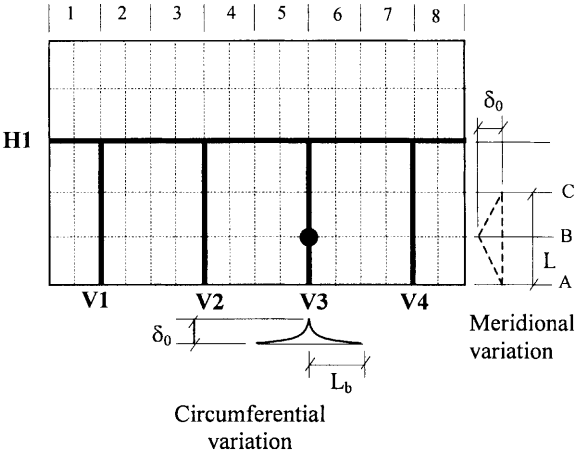

Fig. 3 Bulge variation due to meridional weldment at V3 having a peak at axis B

For demonstration, Fig. 3 shows the circumferential and meridional variation of a bulge resulting from the meridional weldment V3. In this particular figure, the bulge is assumed to be localized around axis B and dies out at axes A and C. Figure 4 shows the variation of a bulge resulting from the same meridional weldment (V3). In this case, two peaks for the bulge are assumed to occur at axes B and C leading to a profile that has constant distribution between the two axes and dies out at axes A and H1. Two bulge cases that might result from the circumferential weldment H1 are shown in Figs. 5 and 6. Figure 5 shows the meridional and circumferential variation of a bulge having a peak value in the middle of segment 6. In Fig. 6, the bulge extends to have a maximum value in the whole length of segment 5 and along half the lengths of segments 4 and 6.

As shown in Figs. 3 to 6, the meridional weldment leads to a bulge having a nonlinear distribution [described by (1) or (2), depending on the assumed type of bulge]

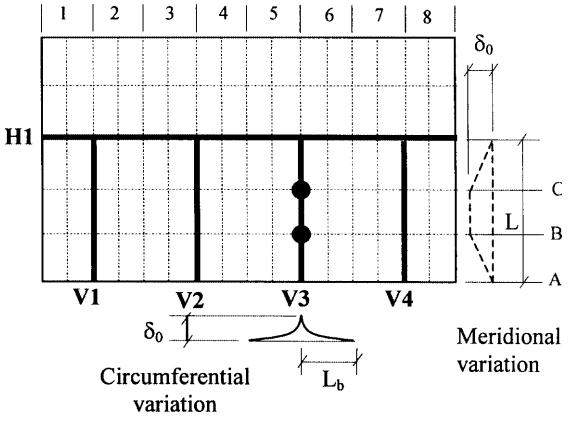

Fig. 4 Bulge variation due to meridional weldment at V3 having its peak between B and C

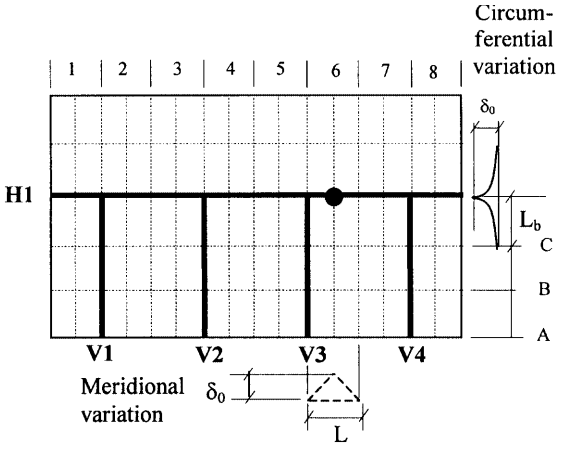

Fig. 5 Bulge variation due to circumferential weldment H1 having its peak in segment 6

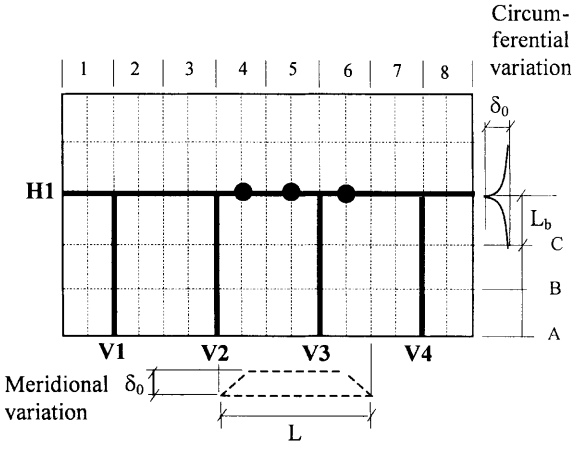

Fig. 6 Bulge variation due to the circumferential weldment H1 having its peak between segments 4, 5 and 6

in the circumferential direction and a linear distribution in the meridional direction. Meanwhile, a circumferential weldment results in a bulge having a nonlinear distribution [described by (1) or (2) depending on the assumed type of bulge] in the meridional direction and a linear distribution in the circumferential direction. The length L_b shown in the nonlinear distribution is defined as the distance at which the ratio δ/δ_0 is almost negligible. In this study, it was decided to choose Lb as the length, from the centre of the weldment, at which $\delta/\delta_0 = 0.005$. The extent in the other direction (the linear distribution) depends on the length of the weldment and the assumed number of segments (n and m)

3 Coupling between shell element model, and binary coded genetic algorithms for critical load identification

The previous section demonstrated how imperfections can be localized on axes and segments along the weldment lines. These localizations divide the weldment lines into discrete segments within which bulges might or might not occur. The occurrence of a bulge at a certain localization can be modelled by a zero-one variable, where zero indicates the nonoccurrence and one indicates the occurrence of the bulge. Figure 7 shows a possible pattern of imperfections along the line of weldments. Each localization has a unique number associated with it, and is represented as a bold line if it has a bulge. The inter-changing occurrence of imperfections, shown in Fig. 7, is only used for demonstration, but any of the 20 weld stretches can be either imperfect or perfect.

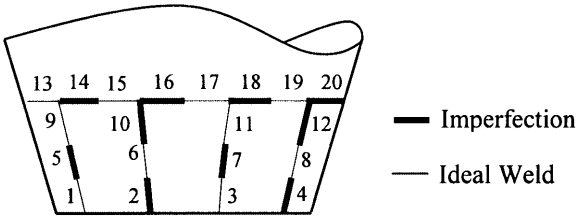

Fig. 7 Sample of imperfection pattern

For the twenty welding localizations between panels, shown in Fig. 7, there can be $2^{20} = 1\,048\,576$ patterns of welding imperfections. It is definitely impossible to conduct such a large number of analyses. Hence in order to find the pattern which gives the limit-buckling load, an optimization method has to be adopted. A typical optimization flow chart for identifying the limit-buckling load is shown in Fig. 8.

The optimization problem at hand falls in the category of zero-one programming problems, where the decision variables assume a value equal to zero or one, and the objective function becomes the minimization of the buckling load. In the presented study, this means that either the bulge occurred at a localization or not. Since the objective function of such problem includes nonlinear finite elements analysis, there is a possibility that the function can be multi-modal. Genetic algorithms (Hadje-Alouane and Bean 1997) have been shown to have good

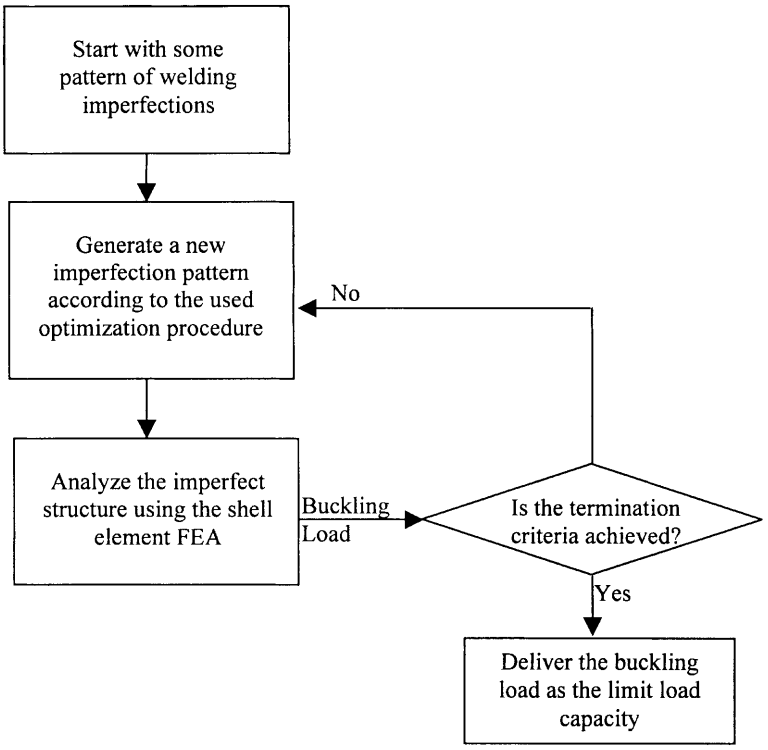

Fig. 8 Flow chart for evaluation of minimum buckling load of thin-walled structures

performance in arriving to near-global optimum solutions if properly coded and if the proper operators are used. Binary coded genetic algorithms are used in this paper to solve the buckling load minimization problem with special choices of operators to suit the problem at hand.

3.1 The finite element model

The finite element model, used in this study, is based on a consistent triangular element that was developed by Koziey and Mirza (1997). The element was extended by Damatty *et al.* (1997a) to include geometric and material nonlinearities. The material model incorporates a strain hardening behaviour and is based on the von Mises yield criterion and its associated flow rule. The inclusion of both types of nonlinearities allows nonlinear stability analysis of shell structures to be conducted using this finite element model. One of the main advantages of this element is being free from the spurious shear models – that lead to a locking behaviour for thin shell problems – associated with isoparametric shell elements. This was achieved by using a consistent formulation that involves a cubic interpolation for displacements and a quadratic interpolation for rotations.

As shown in Fig. 9, the element has a triangular shape and consists of 13 nodes. Ten nodes are used to achieve a cubic interpolation of the global displacement u, v and w, that are directed along the global axes x, y and z, respectively. The rotational degrees of freedom α and β

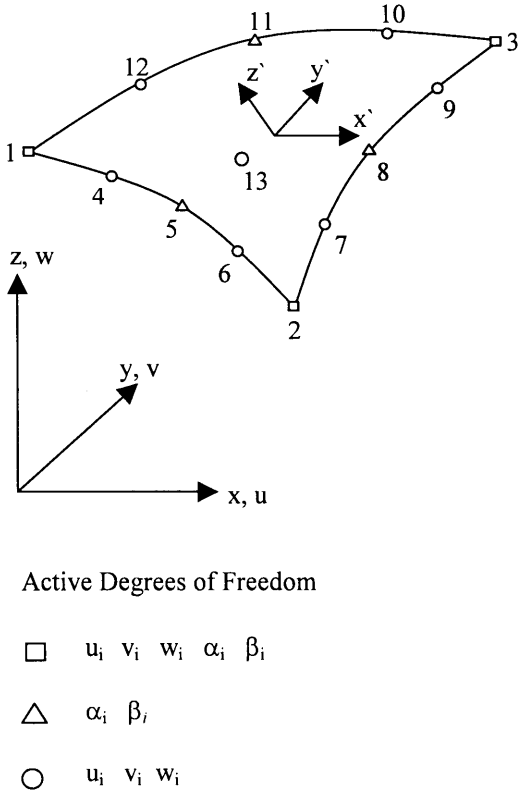

Fig. 9 Coordinates and degrees of freedom of the consistent shell element

are interpolated quadratically using 6 nodes; α and β are rotations about two perpendicular local axes x‘ and y‘, respectively. These axes are located in a plane tangent to

the surface. The geometry within an element is interpolated quadratically by employing the same nodes used to interpolate the rotational degree of freedom.

Since the depression bulge is localized in a relatively narrow region, special attention has to be taken in the finite element model to assure that the quadratic interpolation of the element produces a good description of the bulge geometry. In order to assess the suitable number of elements that has to be used in modelling one side of the bulge, the following steps are conducted.

1. For a certain value of the radius R and the thickness t, (3) can be applied to get the appropriate value of λ.
2. This value is substituted into (1) and (2) to evaluate the function $\delta(x)$ for each one of the bulges (types A and B).
3. One side of the bulge was approximated by either two or three elements. For the case of two elements, two quadratic curves are used to fit the values $\{\delta(0),\ \delta(L_b/4),\ \delta(L_b/2)\}$ and $\{\delta(L_b/2),\ \delta(3L_b/4),\ \delta(L_b)\}$, respectively. For the case of three elements, three quadratic curves are used to fit the values $\{\delta(0),\ \delta(L_b/6),\ \delta(L_b/3)\}$, $\{\delta(L_b/3),\ \delta(L_b/2),\ \delta(2L_b/3)\}$ and $\{\delta(2L_b/3),\ \delta(5L_b/6),\ \delta(L_b)\}$, respectively.
4. The bulge profile (Type A or B) is then compared to the corresponding approximating quadratic function.
5. Steps (1) to (5) are repeated for values of R ranging from 4 to 7 m, using intervals of 1 m, and values of t ranging from 10 to 16 mm, using intervals of 2 mm.
6. Typical plots that show a comparison between the real bulge, the two and three element approximations are shown in Figs. 10 and 11.

The plots shown in Figs. 10 and 11 indicate that at the locations where significant imperfections occur, type A bulge deviates considerably from the two-elements approximation, while being close to the three-elements approximation. As for the type B bulge, both approximations were considerably close to the real bulge. This behaviour was typically shown for the above considered ranges of R and t. As such, it is recommended to use at least two and three elements to model one side of the bulge for types A and B, respectively. In order to identify the restrictions that have to be imposed on the model when simulating an imperfect shell of revolution, a finite element mesh for the typical shell problem discussed in Sect. 2 is shown in Fig. 12.

In view of the above discussion, the following restrictions have to be imposed on the number and the size of the elements, when considering the finite element modelling.

For type A modelling

1. For the three rows of elements adjacent to the meridional weldments, the length of the element in the circumferential direction (L_c) should be less than or equal to one third of the bulge length, i.e. $L_c \leq L_b/3$.
2. For the three rows of elements adjacent to the circumferential weldment, the length of the element in the meridional direction (L_m) should be less than or equal to one third of the bulge length, i.e. $L_m \leq L_b/3$.

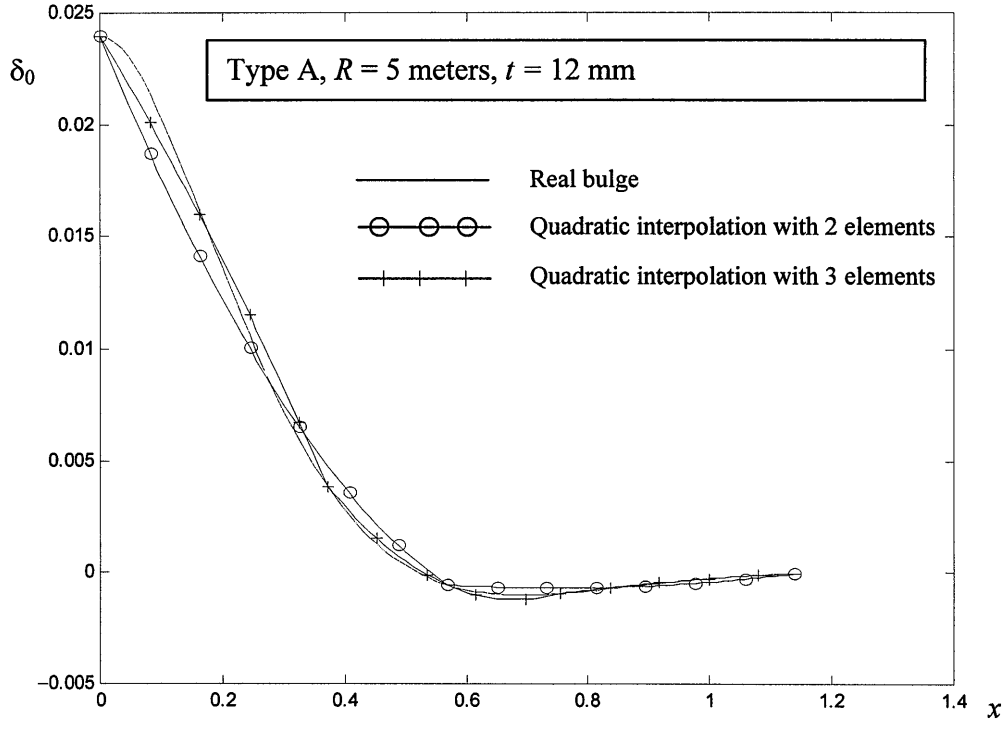

Fig. 10 Comparison between the real bulges and their geometric representation using the finite elements method (Type A)

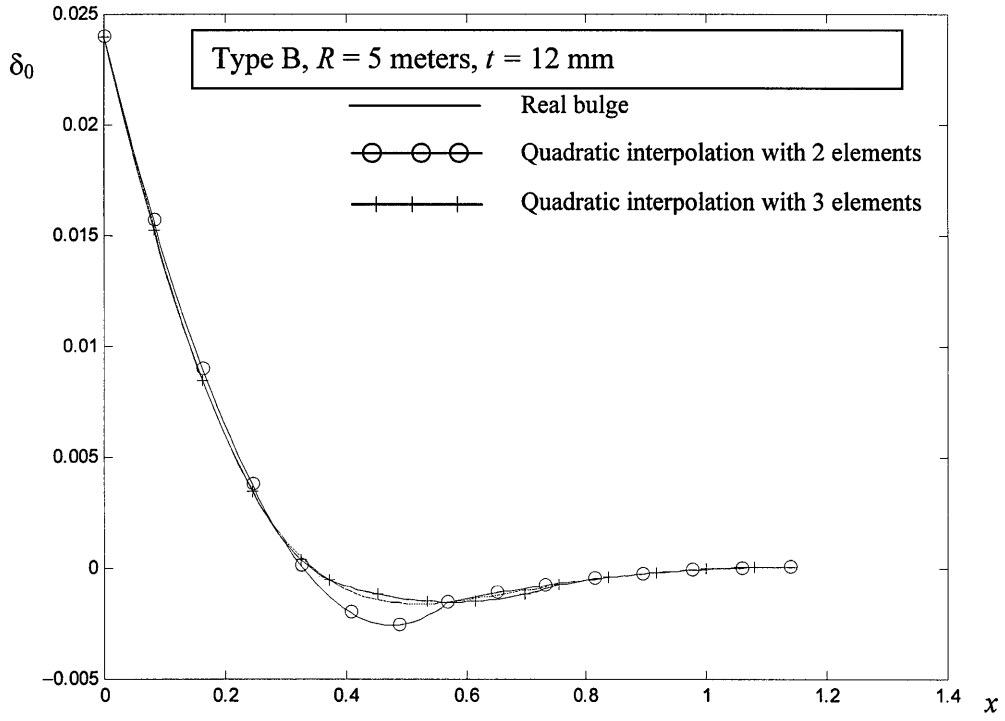

Fig. 11 Comparison between the real bulges and their geometric representation using the finite elements method (Type B)

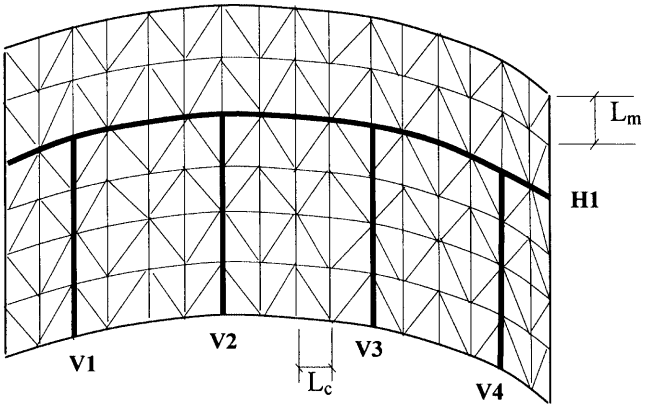

Fig. 12 Finite elements mesh of a thin walled structure with lines of weldments

Fore type B modelling

1. For the two rows of elements adjacent to the meridional weldments, the length of the element in the circumferential direction (L_c) should be less than or equal to one half of the bulge length, i.e. $L_c \leq L_b/2$.
2. For the two rows of elements adjacent to the circumferential weldment, the length of the element in the meridional direction (L_m) should be less than or equal to one half of the bulge length, i.e. $Lm \leq L_b/2$.

For both types A and B modelling

1. In the direction where buckling is anticipated (the meridional and circumferential directions depending on the loading), the lengths of the element Le should be less than one fourth of the wavelength of the buckling mode of the perfect structure (L_r); i.e. $Le \leq L_r/4$, (where, $L_e = L_c$ or L_m).

The first two restrictions are imposed to ensure that the bulge on one side of the weld is properly simulated by the proper number of quadratic functions. The third restriction is to ensure that the finite element mesh detects the first buckling mode.

Once the shell structure is modelled using the appropriate finite element mesh, the solution is carried out incrementally by gradually increasing the magnitude of the load acting on the structure. Iterations are conducted within each load increment using the Newton–Raphson method as described in detail by Damatty *et al.* (1997a). At a certain increment, if the load acting on the structure does not exceed its buckling strength, a convergent solution is achieved (pre-buckling stage). By increasing the load, the stiffness of the structure decreases and the structure reaches its limit load (buckling load) when its stiffness vanishes. Such a limit load can be detected by the finite element model and can happen either in the elastic range (elastic buckling) or after an onset of yielding occurs at some locations of the structure (inelastic buckling).

3.2 Binary coded genetic algorithms

Genetic Algorithms (GAs) are random search methods, which imitate the genetics of natural evolution. During

the process of welding panels of shell structures, the local welding bulge either becomes present or nonpresent depending on the quality control of the welding process. Hence, the problem of identifying the minimum-buckling load of shell structures in the presence of welding imperfections is a zero-one programming problem, where an imperfection between one panel and another is either present or nonpresent. For zero-one programming problems, binary coding is used with the genetic algorithms. Since genetic algorithms operate on sample of solution instances where each instance represents an imperfection pattern, it is important that the solution instances reflect the physical imperfection pattern.

Each instance is composed of a number of locations equal to the number of localized panel weldments. A location can be filled with either 0 or 1; where 0 indicates that the localized weldment is performed ideally, and, 1 indicates that the weldment is associated with an imperfection. Hence, each location refers to a specific localized weldment between a pair of panels. An example of a solution instance and its equivalent pattern of imperfections is shown in Fig. 13.

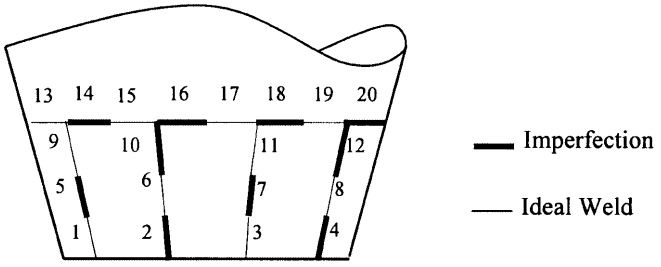

Fig. 13 Example of a solution instance

The general procedure of operation of genetic algorithms is given as follows.

1. Generate a random population of instances
2. $t = 1$
3. while $t \leq t_{\max}$
   (a) evaluate the buckling load $P_{\rm cr}$ associated with each instance
   (b) apply the instance selection scheme
   (c) apply genetic operators (cross-over and mutation)
   (d) replace the population with the new one
4. end while
5. Find the best instance in the final population and deliver it as the problem solution.

The genetic algorithms starts by generating an initial random population $P_0 = \{C_1, C_2, \ldots, C_M\}$ of M instances, where C_i denotes the i-th instance. The pattern of imperfections corresponding to each instance is modelled and the shell structure is analyzed for its corresponding buckling load ${P_{\rm cr}}^i$ using the nonlinear finite elements analysis described in the previous section.

The buckling load values are then used to select instances to be inserted in the consecutive population. First, elitist selection is applied, where the instances with the lowest buckling load is copied to the consecutive population. According to Fogel (1996), this selection ensures the possibility of arriving at the global optimum solution. Using the buckling load values of the first population as a random sample, a geometric distribution of the buckling-loads is estimated, and used to select chromosomes for the application of the following genetic operators.

1. Single point cross-over
   Two instances C_1, C_2 are selected from the population. Both instances are selected at random, where instances with lower buckling loads get higher probability of selection. A bit location j is selected at random and the bit values to the right of the j-th location are swapped between C_1, and C_2.

2. Uniform cross-over
   Two instances C_1, C_2 are selected from the population. Both instances are selected at random, where instances with lower buckling loads get higher probability of selection. For every bit location j, a random variable $b \in [0, 1]$ is generated. If b is less than 0.5, the bit values of the j-th location are swapped between C_1, and C_2, otherwise their original values are retained. This operator is useful with low population sizes, which is needed to decrease the number of the time consuming nonlinear finite elements analysis. (Harik *et al.* 1999).

3. Bit mutation
   A chromosome C_1 is selected from the population. This instance is selected at random, where instances with higher buckling loads get higher probability of selection. A random bit location j is selected and its bit value is reversed.

4. Whole mutation
   A chromosome C_1 is selected from the population. This instance is selected at random, where instances with higher buckling loads get higher probability of selection. For every bit location j, reverse the bit value from zero to one and vice versa. This operator adds an element of uniformly distributed random search at the early iterations, which can be useful in detecting remote global minima. The application of this operator decays exponentially over the iterations.

Note that the cross-over operators are used on good solutions, i.e. ones with low buckling loads. This is needed as cross-over is in a sense a kind of interpolation method between solutions. On the other hand, as mutation operators simulate uniformly distributed random search, they

are applied on low-quality solutions, i.e. instances with high buckling loads. In the numerical examples shown at the end of this paper (Sect. 6), the above set of operators are applied on each population generating the consequent population with the following ratios.

1. Population size = 100 solution instances.
2. 6 instances undergo whole mutation during the initial generations and then that number decreases exponentially to 2 chromosomes.
3. 4 instances undergo bit mutation.
4. 8 instances undergo uniform cross-over.
5. 8 instances undergo single point cross-over.

Each newly generated instance, from any of the above-described operators, is placed in the new population taking the location of an instance randomly selected form the instances of higher buckling loads. In addition, the best instance is also placed in the new population in the location of a high buckling load instance randomly selected form the population. The remaining instances are then directly copied to the new population.

The above procedure is repeated over 40 iterations and the best solution instance in the final iteration is delivered as the problem's solution.

4
Geometric modelling of the imperfect shell structure

The shell structures under consideration in this study are those which fall in the category of surfaces of revolution. Although the study is conducted on cylindrical and conical structures which comprise a wide variety of applications, the same analysis can be extended to general surfaces of revolution.

4.1
Geometric model of the shell structure

Surfaces of revolution are generated, by revolving a general free form curve, called the *generatrix*, around a circle (Fig. 14). If the generatrix is a straight line normal to the plane containing the circle, the surface becomes a cylinder, and, if such a straight line assumes any angle of inclination (other than 90 degrees), a cone is generated. Surfaces of revolution are represented in their most general form using Non-Uniform Rational B-Splines (NURBS). The generatrix can be a general NURBS curve given by the following equation:

$$\mathbf{C}(v) = \sum_{j=0}^{m} R_{i,q}(v)\mathbf{P}_j \,, \tag{4}$$

where, $C(v)$ is any point on the curve corresponding to the independent variable $v \in [0,1]$, $\mathbf{P}_j$: $j \in \{0, \ldots, m\}$ is the set of control points approximating the curve and

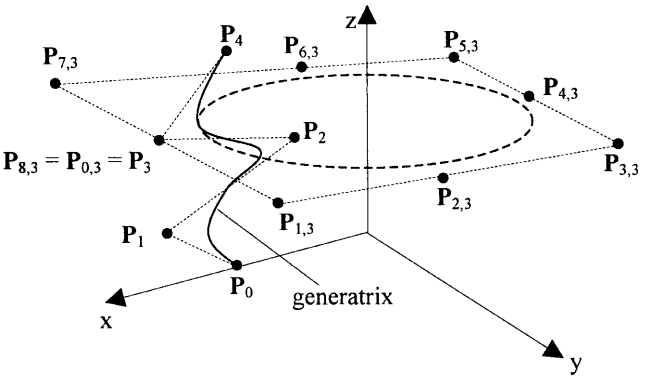

Fig. 14 Surface of revolution

$R_{j,q}(v)$ is the j-th rational B-Spline function of degree q given by the following equation:

$$R_{j,q}(v) = \frac{\mathbf{w}_j N_{j,q}(v)}{\sum_{i=0}^{m} w_i N_{i,q}(v)} \,, \tag{5}$$

where $N_{i,q}$ is the piece-wise continuous B-Spline function, and $\mathbf{w}$ is a vector of weights whose elements range from zero to one. The B-spline function $N_{i,q}$ is defined on a vector U, known as the knot vector, which partitions the domain of the independent variable v into subregions, and consequently causing the spline functions to be nonzero in some curve segments. This property yields the B-spline curve having enough flexibility to be shaped in many arbitrary forms. A more detailed description of NURBS, is given by Piegl and Tiller (1995). The generatrix curve is rotated around a circular curve $\mathbf{G}(u)$, which is also represented by NURBS with the following parameters Piegl and Tiller (1995): $q = 2$, $m = 8$, $\mathbf{w} = \{1, \cos(45),\ 1,\ \cos(45),\ 1,\ \cos(45),\ 1,\ \cos(45),\ 1\}$, $U = \{0, 0, 0, 1/4, 1/4, 1/2, 1/2,\ \ 3/4, 3/4, 1, 1, 1\}$ and the 9 control points take the form of a square (Fig. 14).

Both curves are combined together into one NURBS surface equation

$$\mathbf{S}(u,v) = \sum_{i=0}^{8} \sum_{j=0}^{m} R_{i,2,j,q}(u,v)\mathbf{P}_{i,j} \,. \tag{6}$$

The surface control points $\mathbf{P}_{i,j}$ are generated by revolving the generatrix control points along the path of the circle's control points (Fig. 14). By substituting the proper values for the independent parameters u and v, a cloud of points of the structure can be formed, some of which can be altered to induce the imperfections.

4.2
Modelling of imperfections

Using the cloud of points generated on the surface of revolution, the meridional or the circumferential imperfection

is simulated by applying a displacement normal to the shell structure's surface according to the procedure described in Sect. 2.

5 General procedure

Using the above developed finite element/genetic algorithm model, the procedure to evaluate the minimum buckling load of a thin walled structure follows these steps.

1. The weldment locations (both meridional and circumferential) are identified based on the construction practice.
2. A decision is taken to select a suitable number of bulge segments within the meridional and circumferential weldments.
3. Based on the dimensions of the shell and the bulge length is calculated using (3).
4. A finite element mesh is developed for the problem following the restrictions described in section Sect. 3.1.
5. A value for the amplitude of the bulge δ_0 is assumed (a decision taken based on the level of quality control of the weldment).
6. The genetic algorithm/finite element model is applied to obtain the critical bulge pattern and its associated buckling load.

6 Numerical examples

To illustrate the procedure described in this paper, the numerical optimization model was used to determine the critical imperfection pattern for two thin-walled welded structures. The classical buckling problem of a circular cylinder subjected to pure axial compressive load is studied in the first example. The second example involves the stability analysis of a liquid-filled conical tank. In both examples, type B of bulge patterns was assumed to be associated with the circumferential and meridional weldments. Description of the two problems and results of the analyses are presented in the next subsections.

6.1 Cylinder under pure axial compression load

This example considers a vertical circular cylinder having a radius of $R = 5$ metres, a height $H = 8$ metres and a thickness $t = 12\,\text{mm}$. The cylinder is assumed to be made of steel having a modulus of elasticity $E = 2 \times 10^5\,\text{MPa}$, a yield strength $\sigma_y = 300\,\text{MPa}$, and a Poisson's ratio $\nu = 0.3$. The cylinder is simply supported at both ends and is subjected to pure axial compression load. Assuming symmetry in the longitudinal direction, only one half of the length of the cylinder is considered.

In addition, symmetry about two perpendicular axes located in a horizontal plane is assumed. Thus one eighth

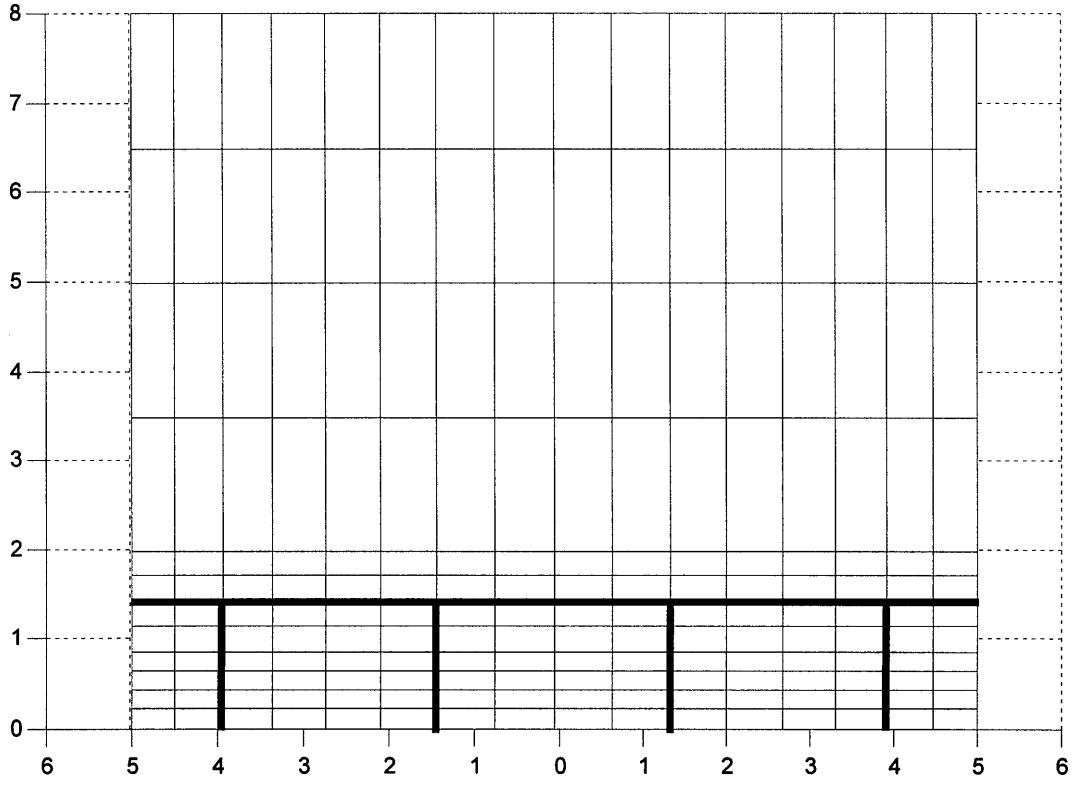

Fig. 15 Finite elements mesh for one quarter of the cylindrical structure

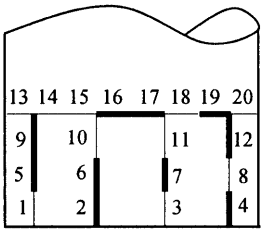

Fig. 16 Critical imperfection pattern and corresponding buckling load

of the cylinder is simulated using the consistent shell element model. The cylinder is assumed to be constructed from a number of panels welded at specified locations. Since buckling is anticipated to occur near the supported edges of the cylinder, only weld depressions that are close to these edges are considered. Based on (3), and using the dimensions of the cylinder, the length of the bulge depression L_b is found to be equal to 0.98 metres. The amplitude of the depression δ_0 was assumed to be equal to twice the thickness of the shell, i.e. $\delta_0 = 24$ mm. This value might be too high in the fabrication process, since according to the API (1987) the permitted imperfection for this case is 9.8 mm.

According to Roark and Young (1982), the buckling wavelength (which is expected to happen near the support) of this classical problem is given by the following relation:

$$\ell_r = 3.44\sqrt{Rt}\,. \tag{7}$$

For the considered case, the above equation leads to a value of $\ell_r = 0.84$ metres. A perspective view of the finite element mesh for one eighth of the cylinder, showing the specified weld locations (4 meridional and one circumferential), is given in Fig. 15. As shown in the figure, a total number of $384 = (16 \times 12 \times 2)$ elements are used. Note that each rectangle in Fig. 15 refers to two triangular shell elements. Based on the dimensions of the cylinder, this finite element mesh satisfies all the requirements given in Sect. 3.1. The assumed number of bulge segments in the meridional (n) and circumferential (m) directions were taken as: $m = 8$, $n = 3$. This leads to a total number of 20 weldments, i.e. 20 decision variables from the optimization point of view.

Based on the geometric and material parameters of the cylinder and according to the equation given by Roark and Young (1982), the elastic buckling load P_{elastic} of this cylinder is equal to 27.3 MN. The dimensionless variable ϕ is defined as the ratio between the buckling load corres-

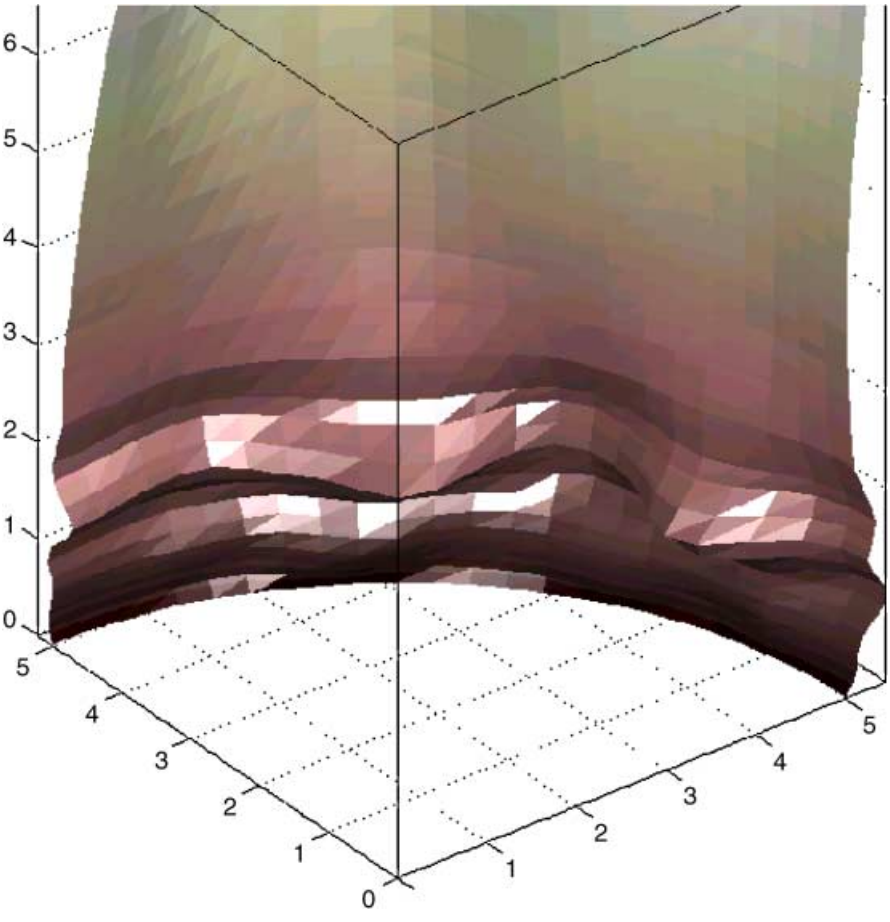

Fig. 17 Buckling mode

ponding to certain imperfection pattern (P_{imp}) and the elastic buckling load of the perfect structure, i.e.

$$\phi = \frac{P_{\text{imp}}}{P_{\text{elastic}}} \,. \tag{8}$$

The minimum value of ϕ, denoted as ϕ_{cr}, corresponds to the critical imperfect pattern. Using the genetic algorithm/finite element model, a minimum buckling load $P_{\text{cr}} = 15.0\,\text{MN}$ was reached leading to $\phi_{\text{cr}} = 0.55$. This result is in agreement with previous experimental evidences (Roark and Young 1982). The critical imperfection pattern corresponding to this critical load is illustrated in Fig. 16, where the solid lines represent the locations along which weld depression occurs. The buckling mode associated with this critical imperfection pattern is shown in Fig. 17, indicating a kind of diamond shape pattern. According to the ECCS recommendations (SSRC 1991, pp. 547–550, 594–597), the critical buckling load of this particular cylinder is 13.9 MN. This result indicates that the above recommendations provide generally a conservative and safe design for cylindrical shells subjected to pure compression.

6.2 Hydrostatically loaded conical tanks

Figure 18 shows a photograph of a typical conical tank. This type of water structures usually consists of a steel conical shell having a superimposed cylindrical shell (composite shell). The steel shell rests on a reinforced concrete tower. In a previous study conducted by Damatty *et al.* (1997b), it was shown that a composite shell can be replaced by a pure cone (by omitting the upper cylindrical part) that has the same volume capacity. Using the same thickness, both structures would have the same buckling capacity. Figure 19 is used to illustrate the state of stresses acting on a conical tank filled with water. The concrete shaft directly supports the weight of the fluid in region II.

Fig. 18 Photograph of a typical elevated conical tank

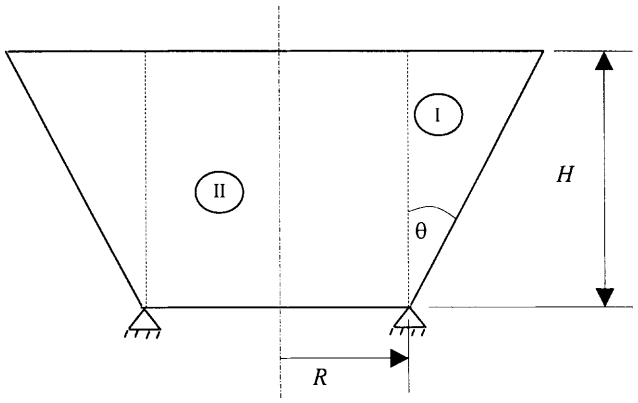

Fig. 19 Conical tank

The weight of the fluid in region I leads to meridional compressive and hoop tensile stresses that are localized at the bottom of the tank.
The compressive meridional stresses are the main cause of buckling of this type of shell structures. These stresses are magnified by local bending resulting from possible geometric imperfections.

A conical tank having a bottom radius $R = 5$ metres, a height $H = 8$ metres, a thickness $t = 12\,\text{mm}$ and an inclination angle $\theta = 45$ degrees, is used as a demonstrative example. The tank is assumed to be simply supported at its bottom edge. Due to the stress concentration and the effect of boundary conditions, buckling is expected to occur at the bottom part of the cone. Hence, the bulges resulting for welds at the bottom region are only considered in the analysis. Symmetry about two perpendicular axes located in a horizontal plane is assumed. As such, only one quarter of the cone is considered.

A perspective view of the finite element mesh used to model one quarter of the cone is shown in Fig. 20 indicating the elements size and the location of the assumed weld lines (shown in bold lines). Note that each rectangle in Fig. 20 refers to two triangular shell elements. Four meridional weldments and one circumferential weldment are assumed in one quarter of the tank. Again, the values of n and m are assumed to be equal to 3 and 8 respectively, similar to the previous example. Also, the magnitude of δ_0 was equal to twice the shell thickness, i.e. δ_0=24 mm. As a result of the variation in the radius, and according to (3), the length of the weld depression (L_b) would vary along the height of the tank. This leads to a value of L_b at the bottom and at the circumferential weld equal to 0.98 metres and 1.15 metres, respectively.

An expression for the buckling wavelength (ℓ_r) of the perfect structure is given by Vanderpitte (1982) which, when applied to this specific problem, leads to $\ell_r = 1.05\,\text{metres}$. Based on the above values of L_b and ℓ_r, the finite element mesh shown in Fig. 20 satisfies the restrictions of Sect. 3.1. The load acting on the tank is carried incrementally by multiplying the specific weight of the fluid by a load factor ϕ. For each analysis (i.e. each

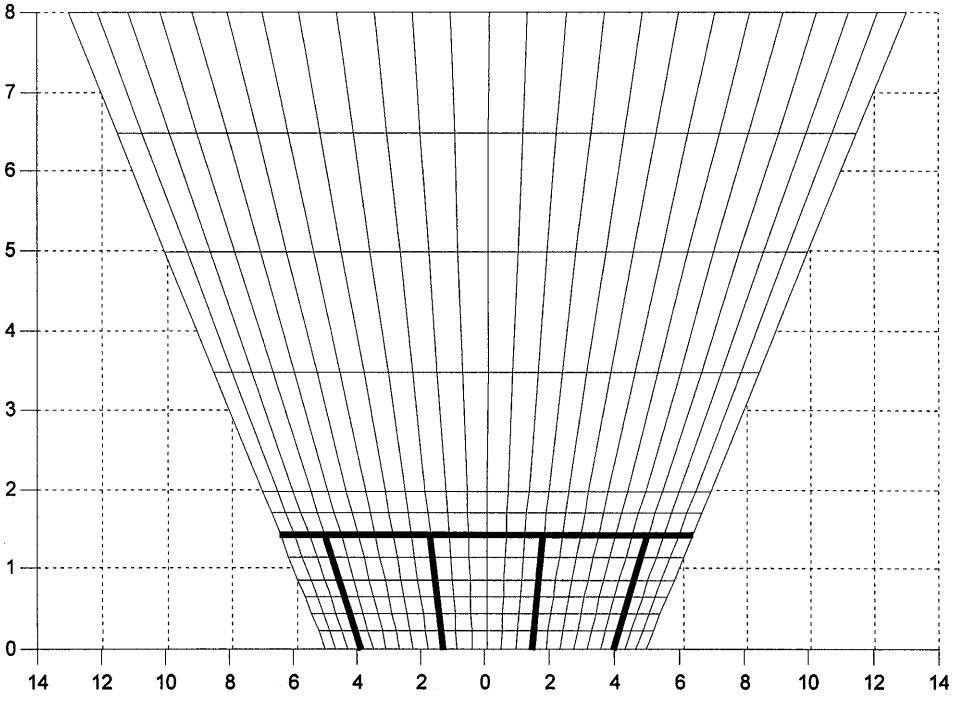

Fig. 20 Finite elements mesh for one quarter of the conical structure

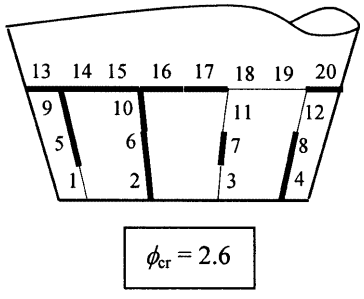

Fig. 21 Critical imperfections pattern for the conical tank

imperfection pattern), the load factor is gradually increased till the structure reaches its limit load at $\phi = \phi_{\text{lim}}$. Analysis was conducted first for the perfect structure leading to ϕ_{lim} (perfect) = 3.0. The optimization technique is then conducted to determine the critical pattern which is illustrated in Fig. 21. The corresponding limit load factor is denoted as ϕ_{cr} and is found to be equal to 2.6.

Compared to the perfect structure, this imperfection pattern leads to a reduction of about 13.3% in the buckling capacity. Previous work by Damatty *et al.* (1997b) indicated a reduction of about 35%, by assuming an imperfection pattern matching the buckling mode of the perfect structure. Meanwhile, the formulae incorporated in the ECCS recommendations (SSRC 1991, pp. 547–550, 594–597), which are based on the research conducted by Vandepitte (1999) lead to a reduction of about 62.5%. As such, one can conclude that the ECCS recommendations provide a conservative design for liquid-filled conical tanks.

7 Summary and conclusions

This paper lays up a procedure that can be used to obtain a practical estimate of the buckling load of thin-walled welded structures. Such a buckling load is greatly affected by the pattern of initial geometric imperfections existing in the structure. In this procedure, a welding configuration for the structure is assumed to be known. Mathematical expressions for the bulge shapes associated with the welding are applied based on previous experimental work. The distribution of these bulges takes a random pattern depending on the quality control of the weldment at various locations. A numerical model is developed in this study to determine the critical pattern of bulges, associated with a certain welding configuration, that leads to the minimum buckling capacity of thin-walled welded structures. The numerical model involves a coupling between the binary coded genetic optimization technique and a finite elements model. The decision variables of the optimization model are the discrete localized weldments; where each local weldment can be either perfect or imperfect, and the critical buckling load is the function to be minimized. The modelling restrictions that have to be adopted in this technique are presented in the study. Two practical examples are applied to demonstrate the methodology. In the first example, the classical problem of buckling of a cylindrical shell under pure axial compressive load is considered. The buckling load associated with the critical imperfect pattern, that resulted from the analysis, coincides with previous experimental evidence. The second problem in-

volves studying the stability of hydrostatically loaded conical tanks. Buckling load obtained from this procedure is compared with the one associated with an imperfection pattern having a wavelength equal to the buckling wavelength of the perfect structure. The comparison reveals that such an assumption of imperfection matching the buckling mode can be overly-conservative and perhaps unrealistic. As such, the suggested procedure based on optimization can provide a more realistic and economical solution.

References

API 1987: *Bulletin on stability design of cylindrical shells*. Wahsington, DC: American Petroleum Institute

El Damatty, A.A.; Korol, R.M.; Mirza, F.A. 1997a: Large displacement extension of consistent shell element for static and dynamic analysis. *Comp. & Struct.* **62**, 943–960

El Damatty, A.A.; Korol, R.M.; Mirza, F.A. 1997b: Stability of imperfect steel conical tanks under hydrostatic loading. *J. Struct. Eng., ASCE* **123**, 703–712

Fogel, D. 1996: *Evolutionary computation: toward a new philosophy of machine intelligence*. IEEE Press

Hadje-Alouane, A.B.; Bean, J. 1997: Genetic algorithms for the multiple choice integer program. *Oper. Res.* **45**, 92–101

Harik, G.R.; Lobo, F.G.; Goldberg, D.E. 1999: Compact genetic algorithm. *IEEE Trans. Evolut. Computation* **3**, 287–297

Koziey, B.L.; Mirza, F.A. 1997: Consistent thick shell element. *Comp. & Struct.* **65**, 531–549

Piegl, L.; Tiller, W. 1995: *The NURBS book*. Berlin, Heidelberg, New York: Springer

Roark, R.; Young, W. 1982: *Formulas for stress and strain* (5th edn.). New York: McGraw-Hill

Rotter, J.M.; Teng, J. 1989: Elastic stability of cylindrical shells with weld depression. *J. Struct. Eng., ASCE* **115**, 1244–1263

Structural Stability Research Council 1991: *Stability of metal structures a world view* (2nd edn.) USA

Vanderpitte, D.; Rathe, J.; Verheddhe, B.; Paridaens, R.; Verschaeve, C. 1982: Experimental investigation of hydrostatically loaded conical shells and practical evaluation of the buckling load. *Proc. State-of-the-Art Colloq.* (held at Stuttgart University, Germany) pp. 375–399

Vandepitte D. 1999: Confrontation of shell buckling research results with the collapse of a steel water tower. *J. Constructional Steel Res.* **49**, 303–314